

# Critical Velocities for Rocket Sled Excitation of Rail Resonance

*James L. Lamb*

**T**he rocket sled test facility at the Holloman Air Force Base in New Mexico provides a unique and valuable test venue for evaluating advanced missile technology at representative flight velocities. Recent failures at the facility underscore the inherent high-risk nature of supersonic sled tests and undermine their potential value to missile development programs. This article addresses one potential cause for some of the observed failures. A periodic structure model of the Holloman test track rail and observed sled response characteristics show that a rocket sled can directly cause the rail to resonate for certain critical sled velocities. The theory is experimentally verified via time–frequency analysis of accelerometer data acquired during sled tests performed for the Navy’s Standard Missile-2 and the Army’s Patriot Advanced Capability-3 missile programs. Both tests culminated in a fractured rail and mission failure. (Keywords: Periodic structure, Resonance, Rocket sled, Wave propagation.)

## INTRODUCTION

APL serves as technical direction agent for the Navy Standard and Tomahawk missile programs and as such participates in planning and executing critical tests designed to evaluate evolving missile system capabilities prior to high-visibility (and expensive) flight tests. The rocket sled test track at the Holloman Air Force Base in New Mexico, the Holloman High Speed Test Track (HHSTT), reproduces aerodynamic flight conditions with high fidelity but also produces an environment of very high vibration. A number of unexplained sled and rail failures have conspired to heighten sensitivity to the high-risk nature of supersonic sled tests. Several critical demonstration programs have not been pursued at the HHSTT because of the inability to mitigate the vibration environment and the risk of payload loss, which experience shows happens too frequently. The high cost and political risks associated with flight tests suggest that rocket sled tests and HHSTT play an increasingly important role in risk reduction of missile systems. A deeper understanding of

the physics underlying the events at the test track will lead to more reliable and more useful experiments.

APL has participated with the Navy and key contractors in numerous sled tests over the years and continues to aid the Navy by assessing the risks associated with future sled tests. One of the dominant risks identified by the author is the potential for dynamic interaction between the rocket sled and the rail upon which the sled rides. The most serious form of interaction arises when the sled impacts the rail so as to directly drive the rail into resonance. Such conditions can arise when the sled reaches certain critical velocities. Since a rocket sled is always accelerating or decelerating, these resonance conditions are excited for only a brief period of time, but the evidence suggests that even brief exposure to resonant or near-resonant amplification is sufficient to cause rail fracture.

This article presents an overview of typical sled tests and the unique features of the test track itself. Under certain circumstances, a sled can directly excite elastic

waves in the rail. The wave propagation characteristics of the 10-mile-long (15.5-km) HHSTT rail are then discussed, and a mechanism whereby the sled can directly cause the rail to resonate is outlined. Finally, the theory of sled-induced rail resonance is confirmed through identification of telltale response features in the time–frequency spectrograms calculated from data obtained from sled-mounted accelerometers during a Navy Standard Missile-2 (SM-2) test and an Army Patriot Advanced Capability-3 (PAC-3) test in which rail fractures occurred and resulted in mission failures. In both cases, the evidence of sled-induced rail resonance was observed to be coincident with the rail fracture event, suggesting that this phenomenon is both real and serious.

## OVERVIEW OF ROCKET SLED TESTS AND SLED–RAIL INTERACTION

Sled tests performed at HHSTT are either a monorail or dual-rail configuration, meaning that the sled either runs on a single rail or is supported between two rails. High-velocity sled tests are usually executed with monorail sleds because of the weight and drag penalties associated with dual-rail sled configurations. Many sled tests require multiple rocket motor propulsion stages in order to accelerate the payload to the desired speeds. The complete system is referred to as a sled train. A typical configuration is shown in Fig. 1. Here, the 1st and 2nd stages are “pusher” sleds, and the 3rd stage is integral with the customer payload (the SM-2 Block IVA forebody in this case). By definition, a pusher sled is not mechanically connected to the sled immediately in front of it, so that when that stage ignites, the drag induced by the blunt forward end of the pusher sled causes it to fall behind the remaining sled train. Some tests require the customer payload to be a separate sled.

The typical configuration in these cases is a four-sled train consisting of three pusher sleds and a fourth unpowered payload sled.

The sled train shown in Fig. 1 is, as is true with most high-velocity sleds, a monorail design. Each sled in the train is attached to the rail by high-strength steel slippers. The slipper effectively wraps around the top portion of the I-shaped rail, leaving approximately a 0.040-in. (0.10-cm) gap all around to allow the sled to slide along the rail. It allows motion along the rail but restrains the sled in the lateral, vertical, and rotational degrees of freedom. One could imagine that a sled slides along the rail top and remains in more or less continuous contact with it for the duration of the test. This is not the case for the high speeds achieved at the HHSTT. Sled motion is best characterized as a combination of free flight punctuated by frequent sled–rail impacts. Sleds bounce; they do not slide.

The HHSTT rail is a unique structure. There are two parallel rails that run in a north–south direction for approximately 10 miles (15.5 km). A third rail runs parallel to these, but is only 3 miles (4.8 km) long. Each rail is fabricated from high-strength steel crane rail segments that are welded together end-to-end to form one continuous rail. The supports, referred to as tiedowns, are equally spaced along each rail for the entire 10-mile (15.5-km) length at intervals of 52 in. (132 cm). Several of these tiedowns are clearly visible in Fig. 1. They provide some degree of translational and rotational restraint to the rail and also serve as a means for achieving and maintaining rail alignment standards.

Following 1st-stage ignition, a rocket sled is exposed to both random and correlated sources of excitation. Random excitation arises from unsteady aerodynamic forces, random fluctuations in rocket motor thrust, and random time intervals between slipper–rail impact events. The impact force is linearly related to the

velocity of impact. This relationship is evident in accelerometer data as a linear dependence of the overall random vibration level on the sled velocity. The random vibration environment to which a sled is subjected can be orders of magnitude worse than the vibration a missile experiences in flight at comparable speeds. For example, the vibration recorded at the guidance section of the simulated SM-2 Block IVA missile shown in Fig. 1 was approximately 32 dB greater than the worst-case vibration experienced by the same section of the missile in flight. This difference is the reason that aggressive vibration isolation schemes are required if

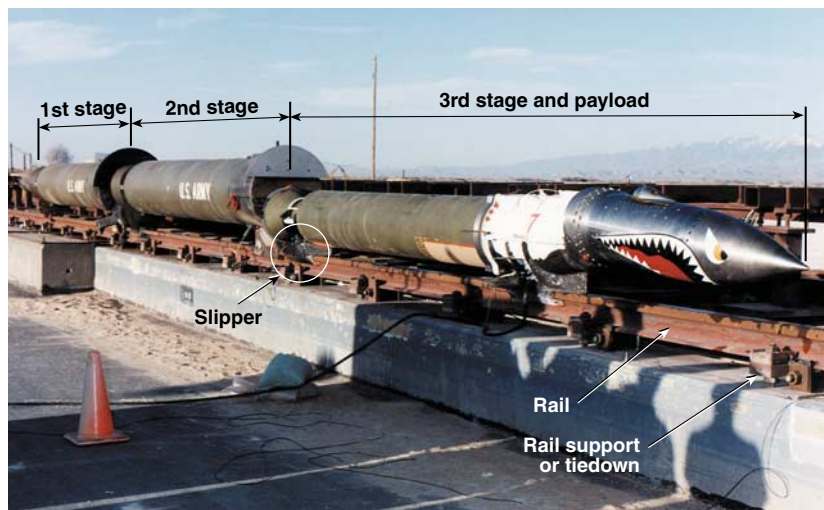


**Figure 1.** Typical monorail sled train (from Standard Missile-2 aerothermal sled test 7).

flight-rated systems are planned for use in a sled vehicle. Unfortunately, if the isolated elements are exposed to the air stream, the significant increase in the aeroshell support flexibility required for vibration isolation tends to render these sleds even more susceptible to aeroelastic coupling and more serious forms of sled–rail interaction, such as sled-induced rail resonance. As a result of the many unknowns and the inherent complexity of sled–rail interaction, HHSTT payload designers discourage the use of vibration isolators.

While it is true that most sleds tend to impact the rail in a more or less random manner, there have been notable exceptions in which a sled has been observed to impact the rail at a well-defined, velocity-dependent frequency. One cause of such behavior may be the highly correlated sources of aerodynamic excitation that act on the sled. Under certain circumstances these forces may act so as to regularize the sled–rail impact events. One form of highly correlated excitation was identified by the author as being a result of vortex shedding.<sup>1</sup> Typically, the surfaces that tend to shed vortices are small enough that the corresponding forces are also quite small. Also, the shedding frequency from small-scale structures (on the order of 1 in. [2.5 cm]) tends to increase so rapidly with sled velocity that the sled cannot be made to impact the rail with the same frequency–velocity characteristics. Vortex shedding does not typically pose a problem for missile-related sled tests.

There is another source of correlated excitation, however, that is believed to be responsible for causing the sled to impact the rail at a well-defined frequency. At supersonic velocities, greater than about 1200 ft/s (366 m/s), a bow shock wave emanates from the tip of the payload aeroshell. The shock wave front is a curved surface, but can be approximated as a conical surface close to the aeroshell. The shock wave represents a discontinuity in the air pressure and density and can reflect off any surface it comes into contact with. The author postulated that the bow shock wave could reflect off the regularly spaced tiedowns and, as a consequence of the fluctuating surface pressures,

give rise to a highly correlated form of excitation of the sled. With the help of the Raytheon Missile Systems Company in Tucson, Arizona, a small surface-mounted pressure transducer was attached to the underside aft-end of the SM-2 payload in an attempt to confirm the presence and document the magnitude of the reflected shock.<sup>2</sup>

The SM-2 payload is shown in Fig. 2a near its peak speed of Mach 4.06. The pressure transducer is located at the position identified as P on the aeroshell. This bow shock cone is shown for two sled velocities, Mach 1.87 and 2.56. The shock cone angle decreases with increasing sled velocity. The location of the rail is delineated with the two parallel white lines drawn on the photograph. Throughout the run, a portion of the

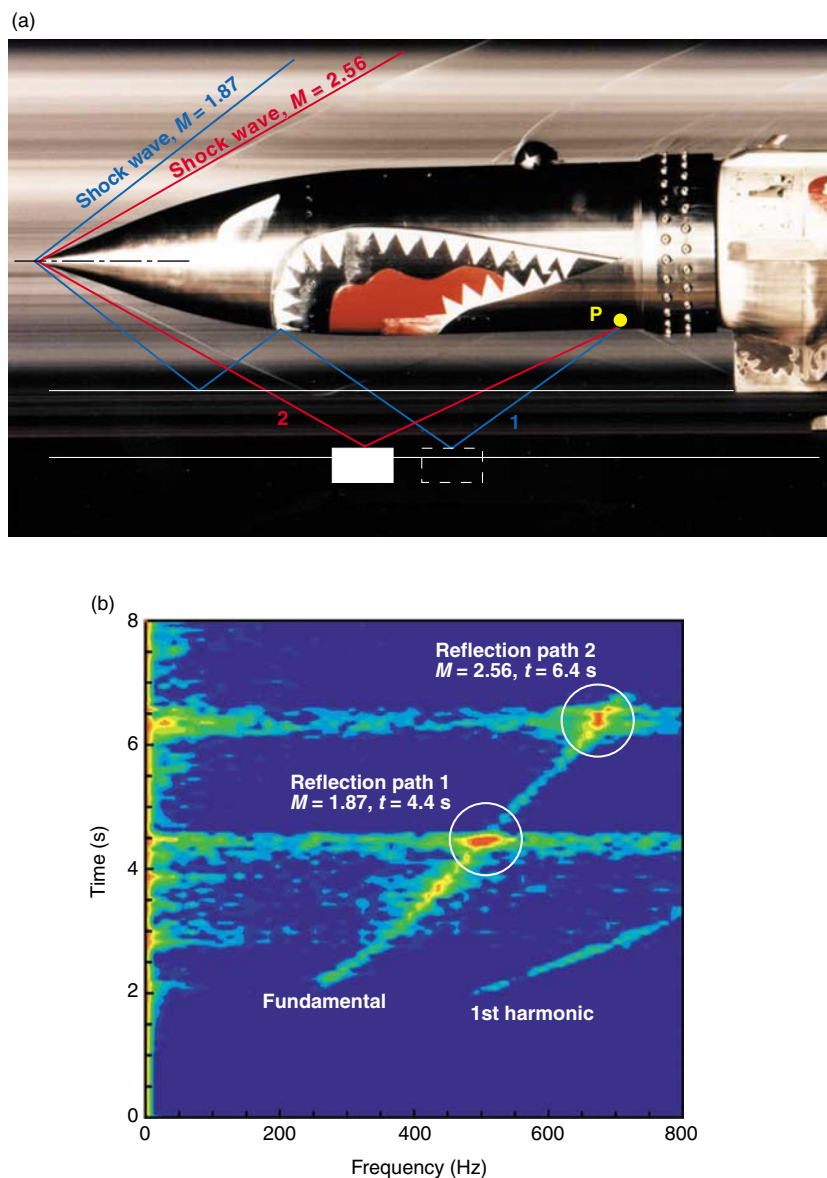


**Figure 2.** Measurement of bow shock reflection off the rail supports. (a) Photograph of the Standard Missile-2 payload ( $M$  = Mach number,  $P$  = pressure transducer); (b) time–frequency spectrogram (pressure data from transducer,  $P$ , above).

shock cone is continuously intersected by the rail and, periodically, intersected by the tiedowns. These hard surfaces reflect the shock waves as shown in the figure. The angle of reflection does not equal the angle of incidence in general.

A time–frequency spectrogram of the recorded pressure signal calculated using the short-time Fourier transform analysis technique is shown in Fig. 2b. The timescale represents mission time  $t$  measured from the initial motion of the sled. Red denotes an amplitude approximately 30 dB larger than the blue. The two diagonal features are caused by the pressure fluctuations produced by the shock reflecting off the periodically spaced tiedowns. Reflection off the continuous top surface of the rail produces only a constant (i.e., zero frequency) pressure shift. The fundamental frequency of the tiedown-reflected shock follows the simple relation

$$f_{\text{shock}} = \frac{V}{L}, \quad (1)$$

where  $V$  is the velocity of the sled and  $L$  is the spacing of the tiedowns.

At Mach 1.87, the shock cone angle is such that the reflection path (path 1, Fig. 2a) causes the impingement point to coincide with the location of the pressure transducer. This event is identified in the time–frequency spectrogram as the significant increase in pressure at a frequency of 500 Hz and recurs for the Mach 2.56 shock cone (path 2, Fig. 2a) at 675 Hz. The reflection signature disappears altogether from the spectrogram after this second impingement incident, as the pressure fluctuations can be sensed by the transducer only when the impingement point is forward of it.

## SLED-INDUCED RAIL RESONANCE

### Theoretical Critical Velocities

Any tendency for one or more of the slippers to impact the rail in a regular manner presents an opportunity for the sled to excite elastic waves in the rail. An elastic wave can be characterized by its propagation velocity  $v_{\text{wave}}$ , wavelength  $\lambda_{\text{wave}}$ , and frequency  $f_{\text{wave}}$ , which have the following relationship:

$$\lambda_{\text{wave}} = \frac{v_{\text{wave}}}{f_{\text{wave}}}. \quad (2)$$

When a sled bounces on the rail with a well-defined slipper-to-rail impact frequency, it theoretically can excite an elastic wave with the same frequency and with

a velocity equal to the sled's velocity. Given this condition, the distance between consecutive slipper impacts is merely the wavelength defined in Eq. 2. The general case of a sled exciting an elastic wave with velocity  $v$  and wavelength  $\lambda$  is illustrated in Fig. 3. In effect, when a sled impacts the rail as shown in the figure, a point on the rail crests just as the sled impacts that point, thereby reinforcing the elastic wave. Clearly, if the sled were to impact the rail at more or less random intervals, no particular elastic wave would be reinforced. The latter behavior appears to be more common.

The discussion of the correlated sources of excitation presented in the preceding section is particularly relevant in the context of the elastic wave excitation mechanism described. While the vortex shedding and shock reflection mechanisms have been measured and identified by APL, there is at least one other mechanism that was recently discovered and remains unexplained (see next section). A summary of the frequency–velocity relationships associated with each of these mechanisms is shown in Fig. 4. If any sled in the train is particularly responsive to any of these driving forces, that sled will tend to excite corresponding elastic waves in the rail. The relationships shown in Fig. 4 therefore represent the elastic waves that can theoretically be excited by a sled.

Some elastic waves that can be made to propagate in the rail have unique properties in that they theoretically can propagate without attenuation when there is no structural damping mechanism present. These are the free, or resonant, elastic waves. Of course some structural damping is always present in any real mechanical system, but the resonant waves are those that can propagate the longest distances before the energy is fully dissipated and that, when directly excited, amplify the input, thus yielding maximum response. An investigation conducted by APL<sup>3</sup> indicates that the level of damping present in the test track is less than 1% of the critical value. These measurements highlight the fact that a disturbance introduced at one point on the track can have a measurable effect much farther

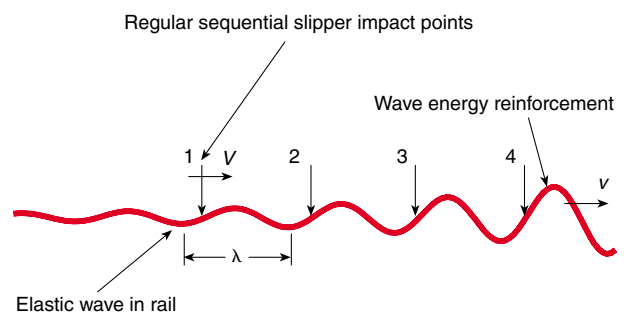


**Figure 3.** Sled excitation of an elastic wave via regular slipper–rail impact ( $V$  = velocity of the sled,  $\lambda$  = wavelength, and  $v$  = velocity of the wave).

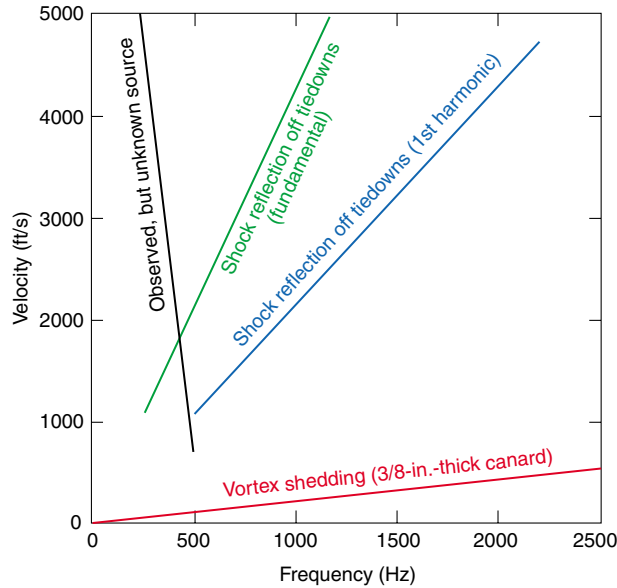


Figure 4. Potential sled-induced elastic waves.

away. This is particularly true for the resonant elastic waves. The possibility that a sled can excite an elastic wave, and a resonant elastic wave in particular, raises the possibility that such a disturbance will travel with the sled and continue to build until the sled excitation differs significantly from the resonant condition. Rail integrity is most susceptible under these circumstances.

The resonant wave characteristics of the rail must be determined in order to identify which of the resonant waves the sled can directly excite. A waveguide such as the HHSTT rail can support many different types of elastic waves. Given the velocity and frequency regime of interest and that the dominant source of excitation acts in the vertical plane, it is the flexural waves that are of most interest in the current investigation. The relevant model for the beam is shown in Fig. 5. The elastic restraint of each tiedown is represented by a translational spring stiffness  $K_T$  and a rotational spring stiffness  $K_R$ . The spring constants were measured in an earlier investigation,<sup>4</sup> and more recent measurements by HHSTT indicate that the stiffness is fairly consistent from one tiedown to the next.

The nature of the construction and the regularly spaced support conditions of the HHSTT rail place it in a unique category of structures known as periodic structures. Furthermore, because of its 10-mile (15.5-km) length, the HHSTT rail may be regarded as an infinite periodic structure. This assumption is reasonable if elastic waves

are unable to reflect off the end of the rail and propagate back to the area of interest with sufficient energy to have an appreciable influence on the response at that location. This is very often the case as the conditions of interest in this article tend to occur several miles from the end of the rail and, though the test track has relatively little damping, a typical disturbance would not be expected to travel more than 2000 ft (610 m). In the current application, the beam vibration characteristics are of most interest, but because of the depth of the rail cross section and the relatively high frequencies of interest, the more complex Timoshenko beam theory, as opposed to the Bernoulli-Euler theory, must be used to identify the resonant flexural waves with acceptable accuracy. The dynamic motion of each periodic element (i.e., each individual 52-in.-long [132-cm-long] span) is governed by the partial differential equation

$$EI \frac{\partial^4 w}{\partial x^4} - \rho I \left( 1 + \frac{E}{G\kappa} \right) \frac{\partial^4 w}{\partial x^2 \partial t^2} + \rho A \frac{\partial^2 w}{\partial t^2} + \frac{\rho^2 I}{G\kappa} \frac{\partial^4 w}{\partial t^4} = 0, \quad (3)$$

where

- $E$  = Young's modulus,
- $I$  = the cross-sectional moment of inertia,
- $w(x,t)$  = deflected shape,
- $x$  = the position within each span,
- $\rho$  = the mass density,
- $G$  = the shear modulus,
- $\kappa$  = the Timoshenko shear coefficient, and
- $A$  = the cross-sectional area.

The right-hand side of the equation is zero because only the free vibration characteristics are of interest in this investigation.

Periodic structure theory basically reduces the analysis effort required for an infinite structure to that

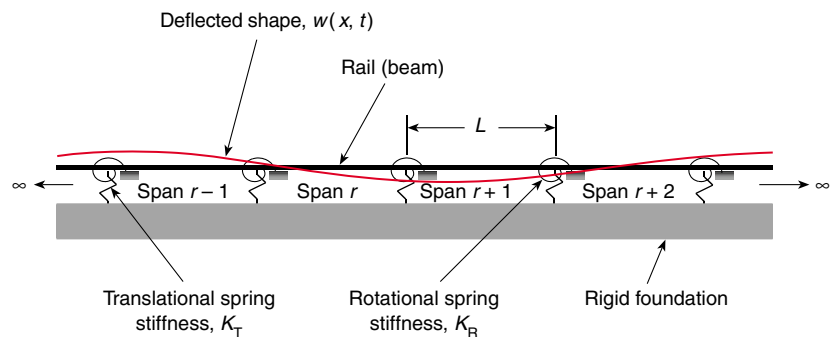


Figure 5. Periodic beam model of the HHSTT rail.

required for a single periodic element. The fundamental principle is based on the relationship that governs the motion of adjacent periodic elements. Specifically, the motion of span  $r$ ,  $w_r(x, t)$ , is identical to that in span  $r + 1$ ,  $w_{r+1}(x, t)$ , but phase shifted according to

$$w_{r+1}(x, t) = w_r(x, t)e^{\mu}, \quad (4)$$

where the phase term  $\mu$  is referred to as the propagation constant and is generally complex and highly dependent on frequency. The relation expressed in Eq. 4 also applies to the internal force components, slope, velocity, and so on.

The governing equation for the propagation constant is given by<sup>5</sup>

$$\begin{aligned} \cosh^2(\mu) + \cosh(\mu)[X_1 \sinh(k_1 L) + X_2 \sinh(k_2 L) - \cosh(k_1 L) + \cosh(k_2 L)] \\ + X_4 + (1 - X_4) \cosh(k_1 L) \cosh(k_2 L) - X_1 \sinh(k_1 L) \cosh(k_2 L) \\ - X_2 \sinh(k_2 L) \cosh(k_1 L) - X_3 \sinh(k_1 L) \sinh(k_2 L) = 0. \end{aligned} \quad (5)$$

The terms  $X_1$  through  $X_4$  depend on the frequency and contain the influence of the support springs:

$$\begin{aligned} X_1 &= \frac{K_T k_1 (k_s^2 + k_2^2)}{2GA\kappa k_s^2 (k_1^2 - k_2^2)} + \frac{K_R (k_s^2 + k_1^2)}{2EI k_1 (k_1^2 - k_2^2)}, \\ X_2 &= \frac{K_T k_2 (k_s^2 + k_1^2)}{2GA\kappa k_s^2 (k_2^2 - k_1^2)} + \frac{K_R (k_s^2 + k_2^2)}{2EI k_2 (k_2^2 - k_1^2)}, \\ X_3 &= \frac{-K_T K_R k_1 (k_s^2 + k_2^2)^2}{4EIGA\kappa k_s^2 k_2 (k_1^2 - k_2^2)^2} - \frac{K_T K_R k_2 (k_s^2 + k_1^2)^2}{4EIGA\kappa k_s^2 k_1 (k_1^2 - k_2^2)^2}, \\ \text{and} \\ X_4 &= \frac{-K_T K_R (k_s^2 + k_2^2)(k_s^2 + k_1^2)}{2EIGA\kappa k_s^2 (k_1^2 - k_2^2)^2}. \end{aligned} \quad (6)$$

In these expressions,  $k_s$ ,  $k_1$ , and  $k_2$  are frequency-dependent wavenumbers determined from the following relations:

$$k_s = \sqrt{\frac{\omega^2 \rho}{G\kappa}},$$

and

$$k_n^4 + k_n^2 \left( 1 + \frac{G\kappa}{E} \right) \left( \frac{\rho\omega^2}{G\kappa} \right) + \frac{\rho\omega^2}{E} \left( \frac{\rho\omega^2}{G\kappa} - \frac{A}{I} \right) = 0, \quad (7)$$

where  $\omega$  is the frequency and  $k_1$  and  $k_2$  are two of the four roots obtained from the second of the two expressions. Two of the roots represent forward-traveling waves ( $k_1$  and  $k_2$ ), whereas the other two roots represent equivalent, but backward-traveling waves ( $k_3$  and  $k_4$ ). The propagation constant can be determined numerically from Eqs. 5–7 for any frequency and is used to distinguish between the resonant and nonresonant elastic waves.

The resonant waves in a periodic structure are those flexural waves that can propagate without attenuation from one span to the next. Nonresonant waves experience a distributed feedback caused by destructive interference, with elastic wave reflections from each successive support. This process manifests itself in the propagation constant. When  $\mu$  is complex, waves cannot propagate from span to span without attenuation; hence, the resonant waves are associated with a purely imaginary propagation constant. The details of this analysis have been carried out using the properties of the HHSTT rail.<sup>6</sup> The propagation constant is found to be purely imaginary over continuous, but finite bandwidths. Separating these regions are other continuous bands in the frequency domain for which the propagation constant is complex. These are the passbands and stopbands, respectively, and are a common feature of infinite periodic waveguides. The resonant waves are confined to the passbands. No elastic wave can propagate far from its source in a stopband.

The resonant wave characteristics for the HHSTT are shown in Fig. 6 together with the observed correlated sources of excitation. The red lines represent all the

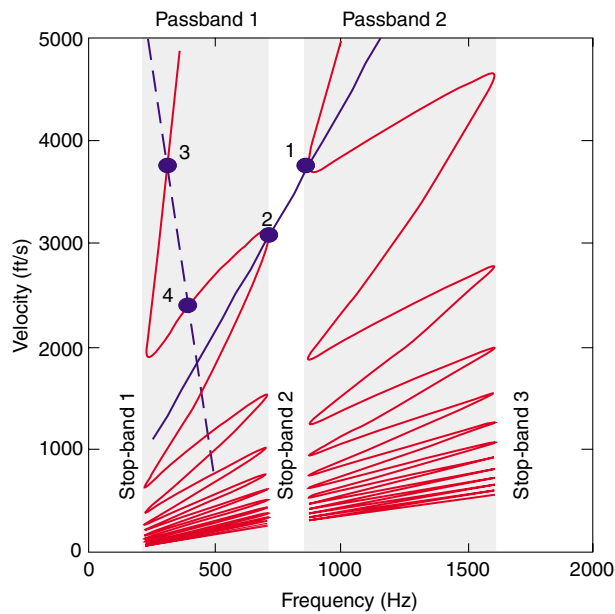


**Figure 6.** HHSTT rail resonance characteristics and potential sled-induced resonance conditions.

possible combinations of resonant wave velocities and frequencies for the first and second passbands (the curves are truncated at the lower-velocity end). The wave velocities are related to the frequency and the propagation constant through

$$v_n = \frac{\omega L}{\text{Im}\{\mu\} \pm 2n\pi}, \quad \text{for } \text{Re}\{\mu\} = 0, \quad n = 0, 1, 2, \dots, (8)$$

where  $\text{Re}\{\mu\}$  is the real part of  $\mu$ . The corresponding wavelengths may be determined from Eq. 2. The resonant waves are confined to well-defined frequency bands as is typical for periodic structures. It is also clear that for a given frequency in a passband, there are many waves (from  $n = 0, 1, 2, \dots$ ), each with a different propagation velocity  $v_n$ . These comprise a resonant wave group. Direct excitation of any one wave in a wave group tends to elicit a large response and also to excite the other waves in the wave group. This feature is not lost on those interested in aircraft noise reduction and detection of underwater marine platforms because external excitation at a specific frequency and wavelength can induce a structural response at the same frequency but at a different wavelength that radiates acoustic energy more effectively.

Only two of the passbands are shown in Fig. 6. There are theoretically an infinite number of passbands; however, at higher frequencies, the Timoshenko beam theory must be discarded in favor of the exact equations of elasticity. The frequency range of interest here is adequately covered by the first two passbands. Also

shown in Fig. 6 are two of the correlated excitation features discussed in the preceding section and plotted in Fig. 4: the dashed blue curve is a shock reflection from an unknown source, and the solid blue curve is the fundamental of the shock reflection off the rail tiedowns. The vortex shedding mechanism and the 2nd harmonic of the shock reflection mechanism have been omitted as they tend to contain far less energy and thus present less of a threat to rail integrity. The intersection of a line representing correlated excitation and a rail passband curve represents a resonant wave that can be directly excited by the sled. The sled velocities at which these intersection points occur are the *critical velocities*. Four resonant wave conditions are identified in Fig. 6. Those at the higher sled velocities are the more serious because the sled impacts the rail with greater force at higher velocities. It is interesting, and probably only a coincidence, that resonance conditions 1 and 3 share the same critical velocity of approximately 3800 ft/s (1158 m/s). The other two conditions identified in Fig. 6 occur at 3070 ft/s (936 m/s) for point 2 and 2330 ft/s (710 m/s) for point 4.

### Experimental Confirmation

Experimental confirmation of the theory outlined here is not a trivial task. First, sled-induced rail resonance does not happen in every sled test. Second, although rail-mounted strain gauges or accelerometers might provide the best documentation of a resonant response of the rail, this approach is problematic because of the expense of such instrumentation efforts, the current inability to predict that resonance will occur, and finally, even though several critical velocities are known, the inability to predict with sufficient accuracy the location on the track where the sled will achieve a particular critical velocity. A practical compromise is to attempt to identify a rail resonance event using the data acquired with sled-mounted instrumentation during a test in which a resonance event is believed to have occurred.

As mentioned, sled-induced rail resonance events are not the norm. Also, most sled tests are performed without telemetry, so the opportunities to confirm the proposed theory are few indeed. Two sled tests have been performed in which the rail fractured and the sled was instrumented with accelerometers. One of these tests was the first of the SM-2 Block IVA aerothermal series performed on 29 July 1994. The other was an Army lethality sled test of the PAC-3 long-body sled performed on 10 June 1998. The PAC-3 test was the second in this developmental series. The earlier test also resulted in a fractured rail at virtually the same sled velocity, but the first sled train was not instrumented. The goals and test hardware of the Navy's SM-2 test series were significantly altered following the 29 July

failure. The Army elected to cancel the PAC-3 test series altogether in the wake of their two failures.

Analyses performed by the author indicate that both rail failure events occurred at the moment the sleds in both tests were simultaneously exciting one of the rail resonance conditions identified in Fig. 6.<sup>7,8</sup> A very restrictive set of conditions must be satisfied before sled-induced rail resonance can be claimed to be the cause of, or a significant contributor to, a rail failure:

- A slipper must be observed, directly or indirectly, to impact the rail at a well-defined frequency.
- The sled velocity and impact frequency must coincide with the velocity and frequency of a resonant wave as defined in Fig. 6.
- The coincidence of velocities and frequencies must occur at the time of rail fracture.

These conditions were met in both the SM-2 and PAC-3 sled tests.

Time–frequency analysis is particularly valuable for identifying the correlated response features—spectral components whose frequencies change with time—discussed here. In order to use the technique for identifying the features shown in Fig. 6, it is necessary to convert the velocity axis into a time axis. This is easily done as HHSTT routinely measures the sled velocity throughout the course of each test using a rail-mounted velocity measurement system. This sled velocity profile can then be used to transform the velocity–frequency rail passband curves into a form suitable for superposition onto a time–frequency spectrogram. This procedure is used for both the SM-2 and the PAC-3 data.

The SM-2 aerothermal test series consisted of nine sled tests, each performed with a three-sled train. The SM-2 forebody was attached to the 3rd-stage rocket motor (Fig. 1). In the first test, the payload was vibration isolated as a prelude to placing an infrared seeker in the aeroshell for subsequent tests. During the test, the 3rd-stage sled caused a rail failure at a speed near 3800 ft/s (1158 m/s). The payload was lost shortly thereafter. The time–frequency spectrogram calculated from an accelerometer positioned near the forward end of the SM-2 aeroshell is shown in Fig. 7. The three diagonal lines (short arrows) are the fundamental and 1st and 2nd harmonics of the shock reflection (Fig. 2) signature. The response as seen by the sled is higher for frequencies outside the first rail passband. A region of low response coincides with the first passband. Also, the high-frequency boundary of the first passband and the low-frequency boundary of the second passband are delineated with higher response. These features result from mechanical feedback from the rail to the sled. In a passband, excitation applied to the rail can be convected away from the source (e.g., a slipper), so the rail acts as a vibration absorber in these zones. In a

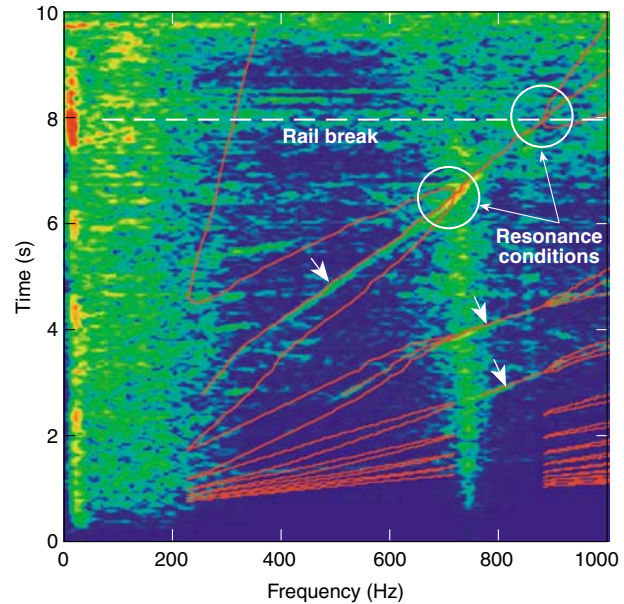


**Figure 7.** Time–frequency spectrogram of the SM-2 aeroshell response.

stop-band, on the other hand, elastic wave energy induced by a slipper cannot propagate away from the source, so the sled senses more resistance and a higher response is recorded.

The passband curves themselves cannot be detected in the response of the sled. Only when a correlated source of excitation directly excites a particular wave on a passband curve is there the potential for any mechanical feedback that can be detected by a sled-mounted accelerometer. Indeed, a very significant feedback event is present at the intersection of the fundamental shock reflection line and the first passband, which coincides with critical velocity point 2 identified in Fig. 6. A corresponding sled response is not measured at critical point 1, but that event does coincide with the moment the rail fracture occurred. This latter point highlights the complexity of sensing rail vibration with an “instrument” as dynamically complicated as the sled while it is traveling at supersonic velocities. Although the absence of a significant feedback event could indicate that the occurrence of the rail failure at that moment was merely a coincidence, it is also possible that the sled was moving in phase with the rail. Maximum feedback would be expected if the sled and rail were moving 180° out of phase.

Alternative explanations have been investigated that might explain the observed response features, but the only other rational one is that they are a result of the sled vibration characteristics themselves rather than the rail. This argument does not hold, however, as APL performed an extensive set of vibration tests<sup>9</sup> on this hardware prior to the sled test and no similar response characteristics were observed. The

only plausible explanation for all of the features observed in Fig. 7 is that the pressure fluctuations from bow shock reflection off the tiedowns caused one or more of the slippers to impact the rail at a very well-defined frequency. In doing so, the sled excited the two rail resonance conditions, giving rise to mechanical feedback to the sled and to an amplified stress state in the rail. In the latter event, which occurred at a sled velocity near 3800 ft/s (1158 m/s), the amplified stress state created by resonance is believed to have caused or contributed to the rail fracture event at approximately 8 s into the test.

A second opportunity to test the proposed failure theory arose in 1998 following the second rail and sled failure in the PAC-3 long body sled test series. This two-test series was performed with a four-sled train: three rocket motor sleds and one payload sled. The first test in the series broke the rail at a sled velocity of approximately 3800 ft/s (1158 m/s). A maximum speed of approximately 6000 ft/s (1830 m/s) was planned. HHSTT staff added several accelerometers to both the PAC-3 sled and the 3rd-stage pusher sled for the second test. The accelerometers were affixed to the three slippers of the PAC-3 (use of a third intermediate slipper is a significant departure from routine HHSTT operations, but was requested by the Army to limit deflections of its rather flexible payload sled) and the two slippers of the 3rd stage. An umbilical was used to ferry the accelerometer wires from the PAC-3 sled back to the telemeter mounted on the 3rd-stage rocket motor.

The telemetry from the PAC-3 was lost approximately 3 s prior to the rail fracture event. The evidence suggests that the telemetry umbilical was adversely affected by the shock wave reflections off the tiedowns.<sup>8</sup> Telemetry from the 3rd stage continued until sled and rail failure. A time–frequency spectrogram calculated from the vertical response of the forward slipper is shown in Fig. 8. Once again, the measured velocity profile was used to transform the relevant curves from Fig. 6 into the time–frequency format suitable for superposition onto Fig. 8.

There is no evidence of the shock reflection signature observed so clearly in the SM-2 test. Still, a signature indicating the presence of a correlated response is visible beginning at 500 Hz, 2–3 s into the test and decreasing to approximately 300 Hz at the time of the rail fracture. Since the signal is dominant and the accelerometer is mounted directly on the slipper, it is reasonable to assume the signal represents the slipper–rail impact frequency. It is surprising that the slipper–rail impact frequency decreases with increasing sled velocity, and the root cause of this behavior remains unexplained. Though this response feature is not as highly correlated as the shock-induced signature observed in the SM-2 test, there still exists the possibility that elastic resonant waves can be excited by it.

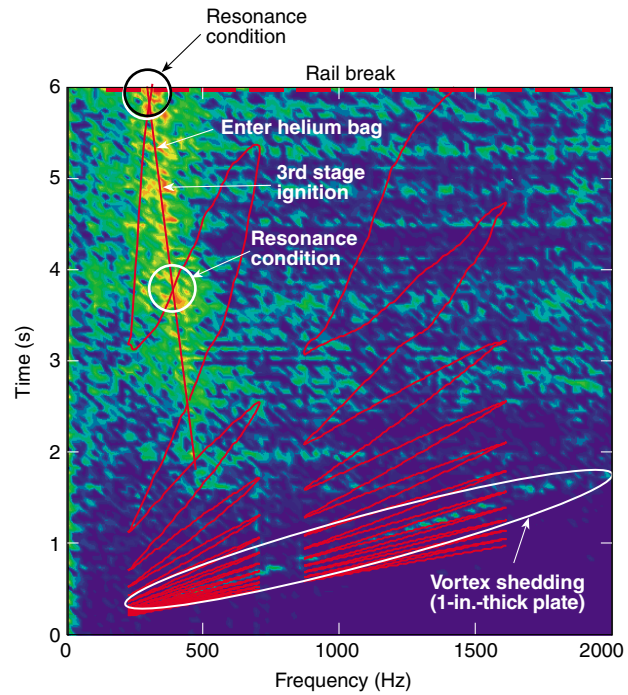


**Figure 8.** Time–frequency spectrogram of the PAC-3 long body 3rd stage, forward slipper.

Several locations along the linear response feature reveal enhanced response, as denoted by localized regions of red in Fig. 8. Two of these occur at 5.0 and 5.4 s and have been identified as being a result of ignition of the 3rd-stage rocket motor and entry of the sled into the helium bag environment, respectively. In order to achieve high velocities with heavier payloads, HHSTT envelops a portion of the rail (typically 1–2 miles) in a helium-filled bag. The reduction in atmospheric density offered by helium translates into reduced drag on the sled. A sled also experiences an abrupt change in acceleration when it enters the helium environment. There is a third event at 4.5 s that has not been correlated with a known source.

In addition to these three events, two other large response conditions are seen. These occur at 3.8 and 5.9 s and coincide with the resonance conditions identified in Fig. 6 as points 4 and 3, respectively. Hence, the data and theory indicate that these response features are a result of sled-induced resonant-mode feedback from the rail. Once again, the latter critical condition occurred at the moment of rail fracture at approximately 6 s into the run when the sled achieved a velocity near 3800 ft/s (1158 m/s). The latter event is particularly serious in that the correlated excitation signature runs virtually parallel to the rail passband curve near the intersection point. This means that the 3rd-stage sled imposed a resonant or near-resonant form of excitation on the rail for a relatively long period of time. Dynamic amplification increases with dwell time.

## SUMMARY

APL has participated in many sled tests in support of Navy missile development and, through its efforts at identifying and reducing the risks associated with supersonic sled tests, has identified dynamic sled–rail interaction as one of the more important and least understood risks. Current sled design procedures at HHSTT do not consider any dynamic interaction between the sled and rail. The rail is assumed to be rigid. The rail resonance theory proposed here and the supporting analyses discussed represent the first attempt to attribute rail failures at the HHSTT as being caused by sled-induced resonance. The periodic beam model was also proposed by the author as a means to evaluate the dynamic response characteristics of the rail. Time–frequency analyses of sled-mounted accelerometer data have proven remarkably useful in identifying rail feedback to the sled at resonant and near-resonant conditions. The presence of resonant-mode feedback confirms both the periodic structure model of the rail and the proposed sled-induced resonance theory. There is still much in the nature of the excitation and response of the rail that is not understood, but the lessons learned thus far indicate that sled–rail dynamics cannot be ignored. This is particularly true in light of the minimal structural damping present in the rail. The small level of damping measured by APL indicates that dynamic disturbances can travel with the sled over very long distances.

The effort to identify potential causes of rail failures is only the first step in reducing the risks associated with hypersonic sled tests. It is also necessary to mitigate the risks associated with sled–rail interaction. The author has recommended the use of continuous tiedown covers over a region of the track as a means of eliminating the periodic reflection of the shock wave off the tiedowns in that region.<sup>10</sup> The covers, which would be approximately 2 miles (3.2 km) long, would be placed alongside the rail at a location on the track where the critical velocities of 3800 ft/s (1158 m/s) and, possibly, 3070 ft/s (936 m/s) would be reached. They would, in effect, “turn off” the correlated excitation during this critical phase, allowing the sled to return to more random contact with the rail and thereby avoiding exciting the resonant waves. Implementation of this solution may have avoided the rail fracture that occurred during the SM-2 test, but probably would not have had any influence on the PAC-3 tests. Further work is required to explain the source of the correlated excitation mechanism observed in the PAC-3 test before a viable approach to mitigating the risks associated with it can be proposed.

Additional rail dynamics studies also should be pursued. The periodic structure theory applied to identify the resonant elastic waves becomes unwieldy when used in the transient response problem (i.e., rail response to a single impact). The ability to accurately predict the response of the rail to a single impact would be valuable in assessing the risk of rail fracture. HHSTT personnel have conducted rail vibration tests using an instrumented impact hammer. These results should be correlated with the corresponding theoretical transient response analysis.

Finally, a better understanding of the interplay among the sled weight, velocity, aerodynamic forces, and the resulting sled–rail impact force is essential. The synthesis of these various tasks will provide much broader comprehension of sled test physics, leading directly to better designed sled vehicles. Ultimately, Army and Navy missile development programs will be able to perform more aggressive and, hence, more useful tests with much lower risk at the HHSTT test facility.

## REFERENCES

- <sup>1</sup>Lamb, J. L., *Vortex Shedding from the Forward Canards on the Rocket Sled Forebody*, Technical Memorandum A1C-98-046, JHU/APL, Laurel, MD (Apr 1998).
- <sup>2</sup>Lamb, J. L., *Measurement of Shock Wave Reflection off Sled Track Tie-Downs*, Technical Memorandum A1C-98-014, JHU/APL, Laurel, MD (Feb 1998).
- <sup>3</sup>Lamb, J. L., *Assessment of Structural Damping in the Holloman Air Force Base High Speed Test Track*, Technical Memorandum A1C-99-020, JHU/APL, Laurel, MD (Feb 1999).
- <sup>4</sup>Graff, K. F., Mahig, J., Wu, T. S., Barnes, R. A., and Kowal, C. R., *Study of Track Failure Criteria*, Department of Engineering Mechanics, The Ohio State University Research Foundation for Air Force Missile Development Center, Holloman Air Force Base, NM (Jan 1966).
- <sup>5</sup>Mead, D. J., “A New Method of Analyzing Wave Propagation in Periodic Structures; Applications to Periodic Timoshenko Beams and Stiffened Plates,” *J. Sound Vib.* **104**(1), 9–27 (1986).
- <sup>6</sup>Lamb, J. L., *Determination of Critical Flexural Wave Speeds in the High Speed Test Track at Holloman Air Force Base*, Technical Memorandum AM-95-E084, JHU/APL, Laurel, MD (Apr 1995).
- <sup>7</sup>Lamb, J. L., *Identification of Sled/Rail Interaction in the Sled Test #1 Payload Response*, Technical Memorandum AM-95-E108, JHU/APL, Laurel, MD (Apr 1995).
- <sup>8</sup>Lamb, J. L., *Evaluation of the Army Patriot Advanced Capability-3 Long Body Sled Test Vibration Data—Implications for Risk in Navy Sled Tests*, Technical Memorandum A1C-99-006, JHU/APL, Laurel, MD (Feb 1999).
- <sup>9</sup>Chang, Y., *Vibration Tests of the STANDARD Missile-2 Block IVA Forebody Simulator*, Technical Memorandum AM-94-E132, JHU/APL, Laurel, MD (Sep 1994).
- <sup>10</sup>Lamb, J. L., *Susceptibility of Flexible Sled Payloads to Sled/Rail Interaction*, Technical Memorandum A1C-98-084, JHU/APL, Laurel, MD (Jul 1998).

ACKNOWLEDGMENTS: The author would like to acknowledge the support of the Navy, specifically Terry Gundersen and Joel Miller, under whose sponsorship this work was performed. The study described herein could not have been undertaken without the valuable experimental data acquired during various sled tests. The help of Larry Mardis and staff of the Raytheon Missile Systems Company and Dave Minto and staff of the HHSTT is also gratefully acknowledged. The author would also like to thank Tim Cowles of the U.S. Army Space and Missile Defense Command for allowing access to the Army sled test vibration data referred to in this article.

THE AUTHOR



JAMES L. LAMB is a member of the Senior Professional Staff in APL's Air Defense Systems Department. He obtained a B.S. in architectural engineering (1983), an M.S. in civil engineering (1985), and a Ph.D. in aerospace engineering (1993), all from the University of Texas at Austin. Dr. Lamb worked as a structural engineer in a consulting firm in Dallas and performed research in the area of structural acoustics at the University of Texas Applied Research Laboratories before joining APL in 1994. Since joining the Laboratory, Dr. Lamb has supported various aspects of the Standard Missile development program. His current areas of responsibility lie in missile system lethality and rocket sled test risk reduction. His e-mail address is [james.lamb@jhuapl.edu](mailto:james.lamb@jhuapl.edu).